YALE PEABODY MUSEUM

JOURNAL OF MARINE RESEARCH

The *Journal of Marine Research,* one of the oldest journals in American marine science, published important peer-reviewed original research on a broad array of topics in physical, biological, and chemical oceanography vital to the academic oceanographic community in the long and rich tradition of the Sears Foundation for Marine Research at Yale University.

An archive of all issues from 1937 to 2021 (Volume 1–79) are available through EliScholar, a digital platform for scholarly publishing provided by Yale University Library at https://elischolar.library.yale.edu/.

Requests for permission to clear rights for use of this content should be directed to the authors, their estates, or other representatives. The *Journal of Marine Research* has no contact information beyond the affiliations listed in the published articles. We ask that you provide attribution to the *Journal of Marine Research.*

Yale University provides access to these materials for educational and research purposes only. Copyright or other proprietary rights to content contained in this document may be held by individuals or entities other than, or in addition to, Yale University. You are solely responsible for determining the ownership of the copyright, and for obtaining permission for your intended use. Yale University makes no warranty that your distribution, reproduction, or other use of these materials will not infringe the rights of third parties.

Hurricane wake restratification rates of one-, two- and three-dimensional processes

by S. Haney[1,2,3], S. Bachman[1,2], B. Cooper[1], S. Kupper[1], K. McCaffrey[1,2], L. Van Roekel[1,4], S. Stevenson[5], B. Fox-Kemper[1,6] and R. Ferrari[7]

ABSTRACT

The restratification of the cold wakes of Tropical Cyclones Fanapi, Frances, Igor and Katrina are examined based on derived scalings for processes that can restore the hurricane wake toward the pre-cyclone conditions. The different restoration processes depend on the parameters of the wake: depth, width, buoyancy anomaly and wind stress. The parameters needed are derived for each wake from satellite and climatological data. The scalings are based on model results and existing parameterizations, including air-sea heat fluxes (one-dimensional) Ekman buoyancy fluxes (two-dimensional) and mixed layer eddies (three-dimensional). The dominant surface restoration occurs by a combination of surface fluxes and Ekman buoyancy fluxes, while the submesoscale mixed layer eddy bolus fluxes are the dominant subsurface effect.

1. Introduction

As a tropical cyclone passes over the ocean, its high winds form a cold wake largely by mixing up deep water to one side of the hurricane eye where the stresses are largest (Price, 1981). The remaining cold wake disappears from the sea surface temperature (SST) typically over a 10-day timescale (Price et al., 2008), but a subsurface bolus of well-mixed water may persist for some time (Mrvaljevic et al., 2013). The cold wake that remains after the passage of a tropical cyclone has been extensively studied for many hurricanes (Ella, Tess, Belle, Eloise, Frances, Fabian, Gloria: Price, 1981; Price et al., 1986; Cornillon et al., 1987; Price et al., 2008). Hurricanes Fabian and Frances have received particular attention because of the Coupled Boundary Layers/Air-Sea Transfer (CBLAST) observational program (D'Asaro et al., 2007; Price et al., 2008; Huang et al., 2009; Zedler et al., 2009; Sullivan et al., 2012).

Some have postulated that hurricane mixing has climatic consequences through a contribution to ocean heat transport (Emanuel, 2001; Pasquero and Emanuel, 2008), although the

1. Cooperative Institute for Research in Environmental Sciences, Boulder, Colorado, USA.
2. Department of Atmospheric and Oceanic Sciences, University of Colorado, Boulder Colorado, USA.
3. Corresponding author *e-mail: sean.r.haney@colorado.edu*
4. Northland College, Ashland, Wisconsin, USA.
5. International Pacific Research Center, University of Hawaii at Manoa, Honolulu, Hawaii, USA.
6. Department of Geological Sciences, Brown University, Providence, Rhode Island, USA.
7. Department of Earth, Atmospheric and Planetary Sciences, MIT, Cambridge, Massachusetts, USA.

magnitude may not be large (Korty et al., 2008; Jansen et al., 2010; Vincent et al., 2012). To affect ocean heat transport, the wake must be deep and persistent enough to exceed the wintertime mixed layer deepening a few months later. Jansen et al. (2010) shows the heat remaining below the permanent thermocline is small and statistically insignificant. Another application of the analysis here would be to predict whether subsequent cyclones passing over the wake might be influenced by a lingering heat content or stratification anomaly of the near-surface ocean. However, these consequences of the wake are of secondary interest. What is of primary interest here is what processes control the recovery of the wake toward pre-cyclone conditions, and how the balance and rates of these processes change depending on the parameters of the wake: buoyancy gradient, depth and width.

The majority of past work has focused on the formation of the cold wakes, rather than their recovery (e.g., Price, 1981; Price et al., 1986; Cornillon et al., 1987; D'Asaro et al., 2007; Huang et al., 2009; Zedler et al., 2009). The primary discoveries are that the wake forms to the right (left) of the cyclone eye in the Northern (Southern) Hemisphere (Price, 1981), as seen in satellite images (Cornillon et al., 1987), and it results primarily from mixing rather than cooling (D'Asaro et al., 2007; Huang et al., 2009; Zedler et al., 2009). An important competition exists between Ekman upwelling and downward mixing during the cyclone (Huang et al., 2009; Zedler et al., 2009). Moderate horizontal resolution and one-dimensional models are better at simulating the formation of the wake than its recovery (Zedler et al., 2009).

This work follows Price et al. (2008), where a one-dimensional model based on Price et al. (1986) (the PWP model), was used to study the recovery of SST after Hurricanes Fabian and Frances based on the local dynamics and surface forcing. They concluded the observed recovery of SST was simulated fairly well by one-dimensional, local processes alone, although they suggest that other processes are likely at play. Thomas and Ferrari (2008) compare a number of different scalings for submesoscale two-dimensional and three-dimensional near-surface restratification and destratification mechanisms of the ocean surface mixed layer, and apply these scalings to idealized model simulations. Here similar scalings for the submesoscale two- and three-dimensional processes are applied to the recovery of the cold wake left behind by the passage of tropical cyclones. The timescale and mechanisms of Ekman Buoyancy Fluxes (EBF: Thomas, 2005) and Mixed Layer Eddies (MLE: Fox-Kemper et al., 2008) are central to the multidimensional recovery process. The wake parameters of different cyclones vary. The investigation here explores whether the recovery mechanisms also vary from cyclone to cyclone.

This work is not intended to improve upon the one-dimensional modeling in Price et al. (2008), but rather to investigate two- and three-dimensional processes, and compare them to one-dimensional restratification. More accurate estimates for these restratification timescales can be achieved in a numerical model, however, including the two- and three-dimensional processes significantly increases the computational expense (over a one-dimensional model) and setup time, and therefore provides a barrier to quickly estimating the restratification timescales for a wide variety of hurricane wake parameters. Thus, the approach here is to develop simple scaling laws to estimate the relative importance of one-,
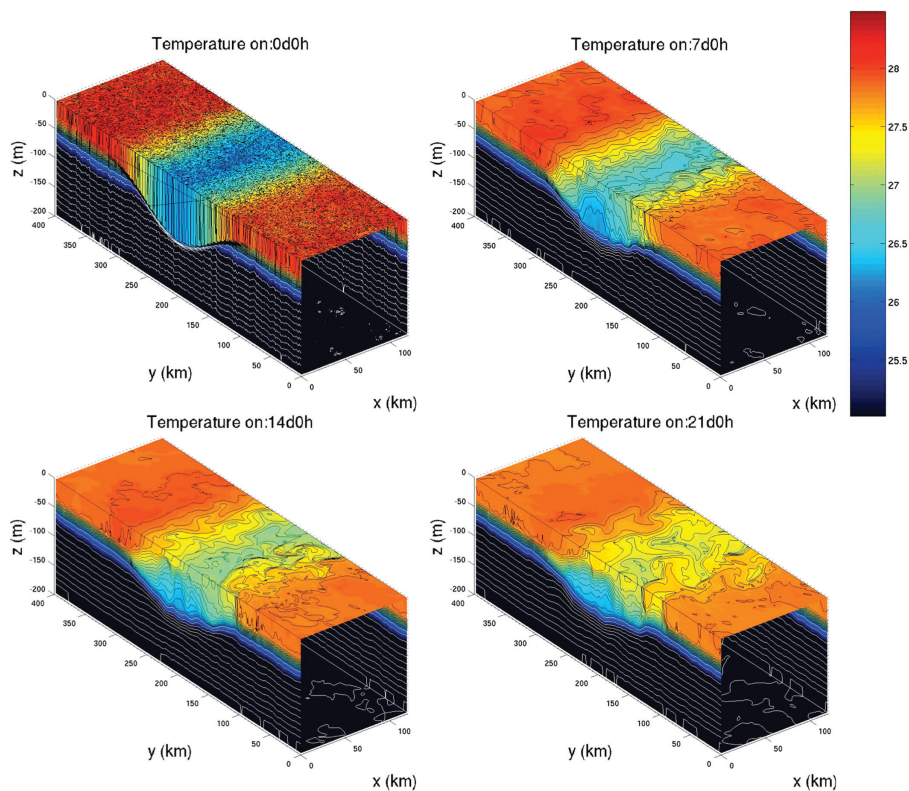
Figure 1. Restratification of an idealized hurricane wake, from initial conditions of a smooth wake plus noise with one snapshot per week. This simulation's parameters (buoyancy gradient, wake depth, etc.) are based loosely on Hurricane Frances.

two and three-dimensional processes, and to evaluate how this relative importance varies across different sets of wake parameters.

A simple methodology for using satellite observations and sub-surface stratification climatologies or profiling floats to estimate the parameters for the wakes of Cyclones Fanapi, Frances, Igor and Katrina are presented. This paper is intended to inform the ongoing analysis of the in situ observations of Typhoon Fanapi and Supertyphoon Megi (Mrvaljevic et al., 2013), future observations of cold wakes by satellite, and the new generation of high-resolution atmosphere-ocean models where tropical cyclone wake restratification is simulated (McClean et al., 2011).

2. An illustrative modeled wake

Figure 1 shows a submesoscale-resolving simulation using the MITgcm (Adcroft et al., 2008) to simulate the restratification of a cold wake based loosely on the parameters and

ambient stratification of Hurricane Frances. The model is helpful to visualize the processes described here. Consistent with the focus on restratification, the wake was initialized as a buoyancy anomaly rather than being mixed by a prescribed wind event. The depth and buoyancy anomaly of the wake were initialized so the stratification outside of the wake is similar to the stratification typical of the region where Frances hit, and the wake was formed by homogenizing the initial conditions from the surface to a sinusoidal depth profile (i.e. temperature contours in the thermocline are sinusoidal inside the wake). The depth of mixing was chosen such that the SST value given in Price et al. (2008) was a result of the deeper mixing rather than a loss of heat to the atmosphere. The same method is used in the scalings discussed in Section 3 to estimate a depth of mixing (described in Appendix A) based on sea surface temperature (SST) images. In the simulation, there is a component of the wind blowing in the x-direction which provides upfront and downfront winds for the two fronts bounding the wake. The simulations were carried out in a 400 km $\times$ 150 km $\times$ 200 m horizontally-periodic domain, with 500 m $\times$ 500 m $\times$ 5 m resolution and a 90 s timestep. The hydrostatic and Boussinesq approximations were used. Salinity was neglected. Temperature was forced with penetrating shortwave radiation and linearized longwave, latent, and sensible heating as described here. A diurnal cycle of nightly cooling and daily penetrating shortwave radiation for Jerlov (1957) water type I was added to the basic forcing, with diurnal cycle fluxes chosen to integrate to zero over the course of a day (as in Fox-Kemper et al., 2008). A two-dimensional (x & y) red noise was added to speed the growth of instabilities. The initial horizontal velocity field was in geostrophic balance with this temperature field, and the initial vertical velocity was zero. The model was run with a monotonic upwind third-order advection scheme without explicit diffusivity and a Smagorinsky viscosity with the coefficient set to one as recommended by Fox-Kemper and Menemenlis (2008).

Four physical mechanisms are apparent in the simulation: EBF, MLEs, geostrophic adjustment, and surface heat fluxes. Figure 2 labels the effects to be discussed. The EBF from the upfront wind restratifies the left-hand front by Ekman transport of light water over dense, and the downfront wind overturns the right-hand front (Thomas, 2005; Thomas and Lee, 2005). The formation of MLEs (Boccaletti et al., 2007; Fox-Kemper et al., 2008; Fox-Kemper and Ferrari, 2008; Fox-Kemper et al., 2011) is apparent by simulation day seven; they form from a red-noise spectrum of temperature anomalies added to the initial conditions and collectively act to extract potential energy from the fronts by tipping them over. A brief period of geostrophic adjustment of the fronts precedes the eddy restratification (Tandon and Garrett, 1994, 1995). However, the geostrophic adjustment results in a horizontal displacement of the surface location of the fronts by approximately one mixed layer deformation radius, which is only a few kilometers compared to the O(100 km) wake opening. The geostrophic wake-bounding currents that result from the adjustment are the precursors of the instabilities resulting in MLE. Surface heat fluxes contribute to a restratification of the near-surface, essentially by the one-dimensional process described in Price et al. (2008). In this simulation the K-Profile Parameterization was used to parameterize surface mixing
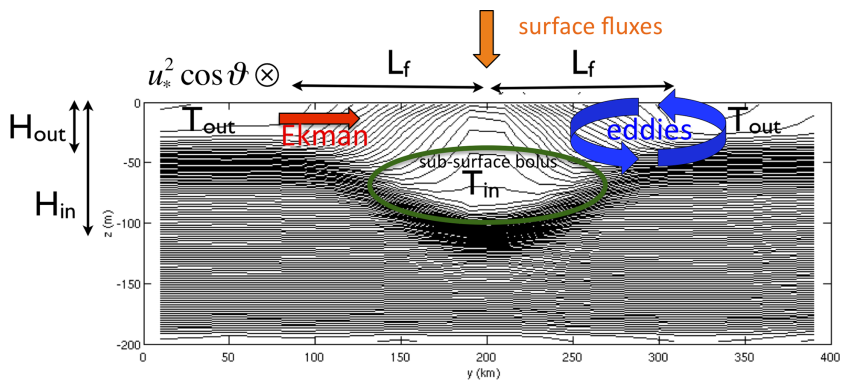
Figure 2. Schematic diagram of cold wake during restratification. The thin black lines are isotherms. Temperatures T_{out}, T_{in}, mixed layer thicknesses H_{out}, H_{in}, front width L_f, and friction velocity squared in the along track direction of the hurricane $u_* \cos \theta$ are indicated. Each restratification mechanism discussed is also depicted, and the region referred to as the sub-surface bolus is shown.

(KPP: Large et al., 1994) instead of the mixing parameterization used by Price (PWP: Price et al., 1986). The heat fluxes are simulated as penetrating solar restratification and latent and sensible heating applied at the surface. The latent and sensible heating is assumed to be proportional to an air-sea temperature difference alone (as is done for the surface flux scaling in Section 3a). Without the wake, these surface fluxes would be balanced (as they are outside of the wake in the simulation). After the cold wake is formed and after the cyclone clouds clear, the solar heat flux approaches its seasonal average, but the latent and sensible cooling are reduced due to the colder SST of the wake, thus a net warming results from the unbalanced surface heat flux terms in the wake.

Note the persistent bolus of well-mixed water from 50 to 100 m depth near the region of deepest mixing in Figure 1. This region experiences mostly eddy restratification, because it lies below the photic zone, and thus below strong solar restratification. Furthermore, this remnant bolus of destratified water is capped over by a stratified layer within a few days of the start of the simulation. Once this stratified upper layer is formed, mixing and convection from the surface are capped, and surface water and momentum can no longer be readily exchanged, eliminating a source of latent and sensible heat to the bolus, as well as trapping the Ekman transport above this stratification.[1]

Baroclinic instabilities of the density fronts on either side of the cold wake form MLEs (Boccaletti et al., 2007). Baroclinic instability requires three dimensions, that is, the along-wake wavenumber must be nonzero for baroclinic instability to occur. Therefore, to remove the effects of MLEs, a matched simulation in two-dimensions otherwise identical to

---

1. The existence of this bolus-capping stratified layer in the model is the basis for assuming in Section 3 that the EBF do not penetrate into the bolus. The formation of this stratified upper layer is an example of the Monin-Obukhov scaling described in Appendix B.
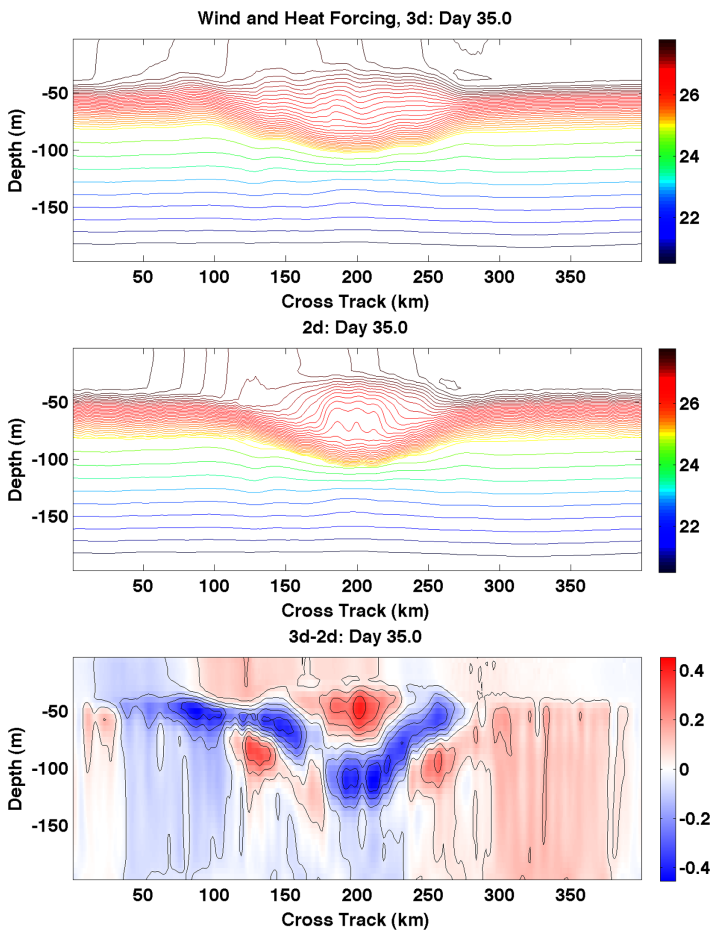
Figure 3. Restratification of an idealized hurricane wake after five weeks. (Upper) Along-wake mean of a three-dimensional simulation with MLEs, wind, and heat forcing, (center) two-dimensional simulation without MLEs, (bottom) difference of the upper two panels, attributable to three-dimensional effects such as MLEs. In the upper two panels, the contour interval is $0.1°C$ in the mixed layer and $0.5°C$ below. The lower panel has a constant contour interval of $0.1°C$.

this simulation was performed and is shown in the middle panel of Figure 3. This two-dimensional simulation includes the same initial density, wind (thus EBF), solar, sensible, latent, Ekman Buoyancy Flux, and Rossby adjustment (Tandon and Garrett, 1994) restratification mechanisms. By comparing the upper (along wake mean of the three-dimensional simulation) and center (two-dimensional) panels of Figure 3, it is apparent that the subsurface bolus has been nearly eliminated by MLEs which spread the thickness anomaly along isopycnals (Fox-Kemper et al., 2008). However, MLEs do not work alone, as they are
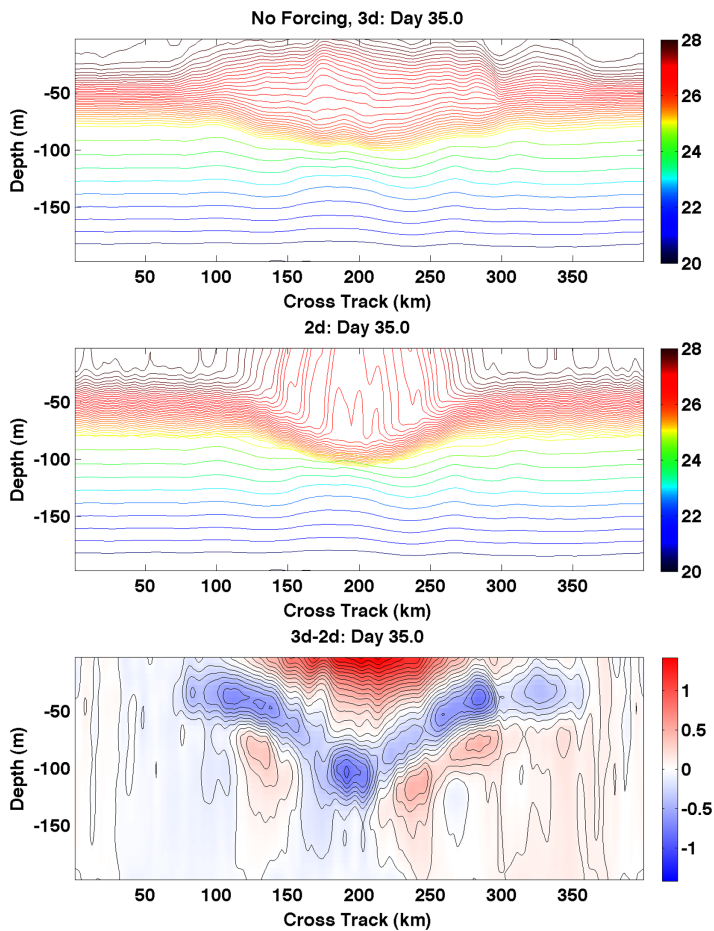
Figure 4. Restratification of an idealized hurricane wake after five weeks, *without* surface fluxes. (Upper) Along-wake mean of a three-dimensional simulation with MLEs, but no wind or heat forcing, (center) two-dimensional simulation with no wind or heat forcing, and without MLEs, (bottom) difference of the upper two panels due to three-dimensional effects such as MLEs. In the upper two panels, the contour interval is $0.1°C$ in the mixed layer and $0.5°C$ below. The lower panel has a constant contour interval of $0.1°C$.

nearly adiabatic as they rearrange water masses, unlike surface fluxes which modify water mass properties. Looking at the bottom panel, the three-dimensional simulation is colder at depth than the two-dimensional simulation, but not warmer near the surface as one would expect if the bolus of mixed water were spread adiabatically by MLEs alone.

Figure 4 further isolates the effects of MLEs. Two-dimensional and three-dimensional simulations are shown with no wind, solar, or surface heating. The only remaining non-MLE

restratification mechanism in the two-dimensional simulation is Rossby adjustment (Tandon and Garrett, 1994), which explains why the isotherms are not purely vertical in the middle panel. The MLEs are nearly conservative when acting on their own. The bolus of mixed water, persistent to the surface even after five weeks in the two-dimensional simulation (middle panel), has been spread out along isopycnals by MLEs in the three-dimensional simulation (upper panel of Fig. 4). However, in contrast to Figure 3, in Figure 4 the two-dimensional and three-dimensional simulations without surface forcing differ by both a cold and a warm anomaly resulting from MLE action (lower panel). The MLEs rearrange water but do not alter heat content. Figure 3 illustrates that the MLEs move warm water upward and cold water downward, but once exposed to the surface the warm anomalies carried by MLEs to the surface are eliminated by heating and cooling. Thus, the net effect of MLEs combined with surface forcing (shown in the lower panel of Fig. 3) differs from the two-dimensional simulation without MLEs only at depth.

The effects of EBF are detectable as well, since all other effects have a mirror symmetry about the center of the wake, while EBF displace the fronts in the direction of the Ekman flow (Fig. 1). The upper panel of Figure 3 shows substantial asymmetry between the fronts. The bottom panel of Figure 3 reveals that there is an interaction of the EBF and MLE effects as well, as also seen by Mahadevan et al. (2010). The sense of the interaction on the left-hand front in Figure 3 is for the EBF to overturn the front–dense over light–rather than restratify it, which results in EBF competing against MLEs in the surface layer. On the right-hand front, MLEs and EBF combine to restratify. Mahadevan et al. (2010) suggest that competition between MLE and EBF strengthens MLEs, while MLEs are inhibited when working together with EBF to restratify. In the deep bolus, given more potential energy from the destratifying downfront winds, MLEs eliminate the subsurface bolus more quickly underneath the left front. The left-right asymmetry is much weaker without winds in Figure 4.

The subsurface cooling attributable to three-dimensional restratification processes in the lower panels of Figures 3–4 is comparable in magnitude. This suggests that the various two- and one-dimensional diapycnal mechanisms (solar, mixing of surface heating, etc.), do not play a leading role in the recovery and spreading of this deeper warm anomaly. However, the agreement between the upper two panels of Figure 3 in the near surface suggests that the eddies have little net effect on recovery of the upper waters. Obviously the degree to which these statements are true will depend on the particular setting of the hurricane wake. The following sections make an attempt to scale the various mechanisms as functions of the wake parameters to anticipate which effects will be dominant.

3. Scalings for hurricane wake restratification

Many restratification mechanisms are at play in the wake recovery process, but each differs in dependence on the parameters of the wake and center of action. In this section

Table 1. Table of values for cold wakes used in this study as estimated from data, showing temperatures T_{out}, T_{in}, mixed layer thicknesses H_{out}, H_{in}, front width L_f, and friction velocity in the along track direction of the hurricane $u_* \cos\theta$. Note, the dates reflect when the wake is first visible in satellite SST images, rather than the date that the hurricane was at that physical location.

Cyclone	Fanapi	Frances	Igor	Katrina	Model
Date	9/19/2010	9/02/2004	9/19/2010	9/04/2005	N/A
Location	22.5N 127.5E	20.4N 61W	22.4N 57.5W	26.4N 86W	22N
$T_{in}(°C)$	$26.3 + 0.6$	$26.72 + 0.08$	$25.63 + 0.06$	$28.1 + 0.2$	26.3
$T_{out}(°C)$	29.37 ± 0.05	28.35 ± 0.04	28.36 ± 0.08	29.44 ± 0.06	27.9
$L_f(km)$	260^{+50}_{-40}	280 ± 60	20^{+20}_{-40}	160_{-30}	100
$u_*^2 \cos\theta (10^{-5} m^2/s^2)$	8 ± 6	8 ± 3	8 ± 4	7 ± 7	4
$H_{out}(m)$	55	30	26	15	30
$H_{in}(m)$	163	120	160	89	110

the timescales and stages of restratification for each of these mechanisms are estimated as functions of the size and strength of the hurricane wake.[2]

Figure 2 schematizes the wake, giving the relevant properties needed for the scalings. Table 1 gives the parameters as estimated for the cyclones studied, including the the modeled hurricane wake described in Section 2 The data collection methods are described in Appendix A.

a. Restratification by solar, infrared, latent, and sensible heat fluxes

If it is assumed that the climatological fluxes are in balance and the temperature outside the wake is indicative of average climatology, a balance equation for the heat content of the mixed layer is approximated as

$$\rho C_p H_{out} \frac{\partial T_{out}}{\partial t} = -Q_{out} + S_{H_{out}}^0 = 0, \tag{1}$$

where solar heat flux divergence is exponential with a decay scale based on wavelength,

$$S_{z_1}^{z_2} \equiv \int_{-z_1}^{-z_2} \frac{\partial}{\partial z}[S_0(I_1 e^{k_1 z} + I_2 e^{k_2 z})]\, dz = S_0 \left[I_1 e^{k_1 z} + I_2 e^{k_2 z}\right]_{-z_1}^{-z_2},$$

thus,

$$Q_{out} = S_{H_{out}}^0.$$

---

2. It should also be noted that there are likely to be currents and eddies–submesoscale or mesoscale–before the hurricane passes over that also advect and stir the cold wake. As the scaling for stirring by these eddies is relatively independent of the parameters of the cold wake, these preexisting eddies will not be treated here, although they are often apparent in SST snapshots of the cold wake (Price et al., 2008; Mrvaljevic et al., 2013).

Here, S_0 is the surface irradiance (taken to be 200 Wm^{-2}), and Q_{out} is the sum of surface latent and sensible heat and outgoing longwave radiation. A dual band exponential form is used for the penetrating shortwave radiation. A Jerlov subtropical water type is used ($I_1 \equiv 0.58$, $k_1 \equiv 0.35\,m^{-1}$, $I_2 \equiv 0.42$, and $k_2 \equiv 23\,m^{-1}$). These penetration parameters may be slightly in error depending on location (e.g., Gnanadesikan and Anderson, 2009), but it is not expected that a small change in the penetration depth of shortwave radiation will have a dramatic impact on the restoring timescale and in any case regional values may be easily adopted for greater accuracy.

Following the work of Large and Yeager (2012), the surface heat flux inside the wake (Q_{in}) can be approximated as a linear perturbation to Q_{out}.

$$Q_{in} \approx Q_{out} + C_{sst}(T_{in} - T_{out}), \tag{2}$$

Then, an equation for the heat content of the cold wake is given as

$$\rho C_p H' \frac{\partial T_{in}}{\partial t} = -Q_{out} + C_{sst}(T_{out} - T_{in}) + S_{H'}^0, \tag{3}$$

where $C_{sst} = \frac{dQ}{dT}|_{T_{out}} \approx 50 \pm 10\ Wm^{-2}K^{-1}$ near the wakes of the cyclones addressed here (Large and Yeager, 2012). A general H' is used in place of H_{in} as the recovering layer depth, since the surface fluxes and EBF affect a shallower portion of the upper ocean as the model results of Figure 3 (center) indicate. If $H' = H_{out}$ then one can see (3) is the balanced Equation (1) with the addition of a linear perturbation $C_{sst}(T_{out} - T_{in})$ that represents the reduced ocean to atmosphere heat flux over the cold wake. In principle, the value of H' should also evolve with time, but here the simpler approach of using a constant value is taken as approximate. By bounding the value of H' above and below, upper and lower limits for restratification time are obtained. Typically, the values H_{in} and H_{out} provide reasonable bounds. A more thorough discussion of the various depths that one could use for H' is in Appendix B.

At the time of year when tropical cyclones are most common, the latent, sensible, and net infrared heat fluxes are usually into the atmosphere, and these fluxes energize the cyclone. Despite the cold wake being significantly colder than the undisturbed ocean, it is still warmer than the atmosphere. Therefore, the perturbation to the surface flux (latent, sensible and net infrared radiation) proportional to C_{sst} in (3) is still smaller in magnitude than Q_{out} which cools the wake. The penetrating solar radiation term in (3) always heats the cold wake, but to a greater or lesser degree depending on the depth of the wake compared to the solar penetration depth. Therefore, the shortwave radiation that penetrates below the restratifying layer acts on the deeper bolus. The final temperature to which the cold wake can warm to (T_f) is determined by considering (3) in the steady case.

$$T_f = T_{out} - \frac{1}{C_{sst}} S_{H'}^{H_{out}} \tag{4}$$

For $H' = H_{out}$, T_f is simply T_{out}.

To give a timescale for restratification by solar fluxes (τ_{sf}), (3) is integrated from T_{in} to the e-folding temperature anomaly relative to T_f, $\left(T_f - \frac{T_f - T_{in}}{e}\right)$,

$$\int_0^{\tau_{sf}} \partial t = \rho C_p H' \int_{T_{in}}^{T_f - \frac{T_f - T_{in}}{e}} \frac{\partial T_{in}'}{-Q_{out} + C_{sst}(T_{out} - T_{in}') + S_{H'}^0}$$

$$\tau_{sf} = -\frac{\rho C_p H'}{C_{sst}} \ln \left(\frac{C_{sst}\left(T_{out} - \left(T_f - \frac{T_f - T_{in}}{e}\right)\right) - S_{H'}^{H_{out}}}{C_{sst}\left(T_{out} - T_{in}\right) - S_{H'}^{H_{out}}} \right)$$

$$= \frac{\rho C_p}{C_{sst}} H'. \tag{5}$$

Coincidentally, $\frac{\rho C_p}{C_{sst}}$ turns out to be almost exactly the conversion factor from seconds to days, so

$$H'(\text{in meters}) \approx \tau_{sf}(\text{in days}).$$

Note that shallow and deep H' differ in that shallower layers evolve to a colder T_f given by (4). In these cases, for a complete recovery to the climatological stratification and T_{out}, other processes must also evolve the depth to H_{out}, which takes somewhat longer than the timescale estimated here.

i. Solar Heating in the Sub-Surface Bolus The subsurface bolus (between $-H_{in}$ and $-H'$) of anomalously warm water returns to pre-hurricane temperatures much more slowly than the thin surface layer (above $-H'$). Motivated by the model results (Fig. 3, center), it is assumed that this sub-surface layer is too deep to be affected by EBFs, therefore, the only restratification mechanisms affecting it are penetrating solar radiation and MLEs. The shortwave solar radiation that penetrates to this layer is given by $S_{H_{in}}^{H'}$, and a timescale for solar restratification in this layer is the heat content anomaly of the layer divided by the heating rate

$$\rho C_p \frac{(H_{in} - H')(T_{out} - T_{in})}{S_{H_{in}}^{H'}} = \tau_{sb}. \tag{6}$$

b. Modification of stratification by EBF

The cold wake may be restratified by the cross-frontal Ekman transport, or EBF. The induced Ekman flow can stratify or de-stratify the wake depending on the orientation of the surface wind stress. If the wind is blowing up-front (i.e., opposing the thermal wind shear), the Ekman flow will transport lighter water over denser to flatten the isopycnals and restratify. In the case where the winds are blowing down-front, the Ekman flow will steepen the isopycnals, overturning and reducing the stratification within the wake. Since

the Ekman flow is given by $\frac{u_*^2}{f\delta}$, where δ is the Ekman layer depth and f is the Coriolis parameter, a timescale for restratification can be written as

$$\frac{\text{wake width}}{\text{Ekman Flow}} = 2\frac{L_f f H'}{u_*^2 cos\theta} = \tau_{ebf}, \qquad (7)$$

where θ is the relative angle between the wind stress and the hurricane track direction and it is assumed that $\delta = H'$, consistent with the restratifying layer limiting the depth of turbulent momentum transport. The vertically integrated Ekman transport is considered here rather than the Ekman spiral. In the simulations discussed in Section 2, turbulent momentum transport varies substantially due to KPP, which makes the Ekman spiral nontrivial to estimate. Furthermore, turbulent and convective mixing frequently homogenizes the water masses displaced by the EBF mechanism, so the bulk Ekman transport seems appropriate for the net process, following Thomas (2005).

c. Modification of stratification by MLEs

Fox-Kemper and Ferrari (2008) propose a parameterization for the restratification rate by MLEs based on the parameters of the density front on which they form. The MLE parameterization is given by

$$\mathbf{\Psi} = C_e \frac{H_{eddy}^2 \nabla \overline{b}^z \times \hat{\mathbf{z}}}{|f|}\mu(z), \qquad (8)$$

$$\mu(z) = \max\left\{0, \left[1 - \left(\frac{2z}{H} + 1\right)^2\right]\left[1 + \frac{5}{21}\left(\frac{2z}{H} + 1\right)^2\right]\right\},$$

where $H_{eddy} \approx \frac{1}{2}(H_{in} + H_{out})$ is the depth over which the eddies act, f is the Coriolis parameter, b is buoyancy, and $\hat{\mathbf{z}}$ is the unit vertical vector. The overline with superscript z on $\nabla \overline{b}^z$ is understood to be the depth-average of ∇b over the mixed layer. The efficiency coefficient C_e is approximately 0.06 (Fox-Kemper et al., 2008; Bachman and Fox-Kemper, 2013).

The parameterization is cast as an eddy-induced overturning streamfunction ($\mathbf{\Psi}$), which provides an eddy-induced velocity field ($\mathbf{u}^\dagger = \nabla \times \mathbf{\Psi}$). Advection by the eddy-induced velocity provides the eddy fluxes of tracers, including the buoyancy skew flux ($\overline{\mathbf{u}'b'} = \mathbf{\Psi} \times \nabla \overline{b}$). This skew flux is guaranteed to be purely along isopycnals, which is the dominant eddy flux restratification mechanism (Fox-Kemper and Ferrari, 2008).

Applying this parameterization to the hurricane wake restratification problem involves estimating the relevant horizontal buoyancy gradient and the appropriate mixed layer depth. A simplified model of the scenario is shown in Figure 2. To a good approximation, the maximum magnitude of overturning will be

$$\nabla \bar{b}^z \times \hat{\mathbf{z}} \approx (b_{out} - b_{in})/L_f, \tag{9}$$

$$|\mathbf{\Psi}| = C_e \frac{H_{eddy}^2(b_{out} - b_{in})}{L_f |f|} \mu(z)$$

where $(b_{out} - b_{in})$ is the buoyancy gradient due to temperature, $g\alpha(T_{out} - T_{in})$. Appendix D shows that this parameterization is applicable to the adiabatic MLE restratification in Figure 4. $|\mathbf{\Psi}|$ will be centered near the bullseye region in Figure 9.

Given $\mathbf{u}^\dagger = \nabla \times \mathbf{\Psi}$, the surface velocity that is sealing the wake may be approximated by

$$|v^\dagger|_{z=0} = \left| \frac{\partial \mathbf{\Psi}}{\partial z} \right|_{z=0} \tag{10}$$

$$\approx \left| C_e \frac{H_{eddy}^2(b_{out} - b_{in})}{L_f |f|} \frac{\partial \mu(z)}{\partial z} \right|_{z=0}$$

$$\approx C_e \frac{H_{eddy}^2(b_{out} - b_{in})}{L_f |f|} \frac{104}{21 H_{eddy}}.$$

A timescale for surface resealing by eddies can be estimated as the time for warm water from outside the wake to travel L_f at the eddy-induced velocity $v^\dagger$. This is given by

$$\frac{L_f}{|v^\dagger|_{z=0}} \approx \frac{0.2}{C_e g\alpha} \frac{L_f^2 |f|}{H_{eddy}(T_{out} - T_{in})} = \tau_{eddy}, \tag{11}$$

where g is the acceleration due to gravity ($9.81 \ m \ s^{-2}$) and α is the coefficient of thermal expansion ($2.07 \times 10^{-4} \ K^{-1}$). Unlike τ_{sf} and τ_{ebf}, τ_{eddy} gives a surface sealing time rather than the restratification time for a layer of thickness H'. Eddy restratification of a layer of thickness H' can be estimated with the buoyancy skew flux, as in the following two sections, however the surface sealing has been found to be a more robust timescale estimate. The buoyancy skew fluxes are more sensitive to local variations in the vertical and horizontal buoyancy gradients. Differences between the isopycnals produced by the eddy parametrization and by the three-dimensional simulation are shown in Figure 9.

i. Vertical supply of cold water to the bolus by eddies. Restratification of the surface anomaly is not the only effect of eddies, as one might also consider the rate at which they exchange warm water in the sub-surface bolus with cold water outside of the bolus by skew flux along isopycnals. As stated in the previous section, the skew fluxes are more sensitive to local variations in the buoyancy gradients, however in the bolus restratification, there is no analog to the surface sealing time, so skew fluxes are used. It was this metric that was used to argue for climatic impact of MLEs in Fox-Kemper and Ferrari (2008a). This vertical flux is given by

$$\overline{w'b'} = \mathbf{\Psi} \cdot \hat{\mathbf{x}} \frac{\partial \bar{b}}{\partial y} \tag{12}$$

$$\approx C_e \frac{H_{eddy}^2 (b_{out} - b_{in})^2}{L_f^2 |f|} \mu(z).$$

This flux reaches a maximum midway through the mixed layer, where $z = -H_{eddy}$, and $\mu(z) = 1$. Horizontally integrating $|\overline{w'b'}|_{z=-H_{eddy}}$, and comparing to the volume integrated buoyancy anomaly within the bolus provides a timescale estimate for bolus restratification:

$$\frac{\text{buoyancy anomaly}}{\text{vertical buoyancy flux}} = \frac{\int_{-H_{in}}^{-H'} \int_0^{L_f} b' \, dy \, dz}{\int_0^{L_f} |\overline{w'b'}|_{z=-H_{eddy}} \, dy} \tag{13}$$

$$\approx \frac{1}{C_e g \alpha} \frac{(H_{in} - H') L_f^2 |f|}{H_{eddy}^2 (T_{out} - T_{in})}. \tag{14}$$

$$= \tau_{ev} \tag{15}$$

ii. Removal of cold water from the bolus laterally by eddies. Finally, it is useful to estimate the horizontal fluxes out of the deep mixed bolus region. As noted, the skew flux spreading this anomaly will be along isopycnals. A control volume containing the bolus will therefore experience fluxes out of each side. A scaling for these horizontal fluxes is

$$|\overline{v'b'}| = \left| \mathbf{\Psi} \cdot \hat{\mathbf{x}} \frac{\partial \bar{b}}{\partial z} \right| \tag{16}$$

$$\approx C_e \frac{H_{eddy}(b_{out} - b_{in})^2}{L_f |f|} \mu(z).$$

The depth over which these fluxes act is $-H_{eddy}$ to the top of the bolus, therefore, $|\overline{v'b'}|$ is integrated vertically from $-H_{eddy}$ to the top of the remaining buoyancy anomaly $\left(-H' = -\gamma H_{eddy}; \text{ where } \gamma = \frac{H'}{H_{eddy}}\right)$. Comparing these fluxes to the area integrated buoyancy anomaly gives the timescale

$$\frac{\text{buoyancy anomaly}}{\text{horizontal buoyancy flux}} = \frac{\int_{-H_{in}}^{-H'} \int_0^{L_f} b' \, dx \, dz}{\int_{-H_{eddy}}^{-\gamma H_{eddy}} |\overline{v'b'}| \, dz} \tag{17}$$

$$\approx \frac{1}{m(\gamma) C_e g \alpha} \frac{(H_{in} - H') L_f^2 |f|}{H_{eddy}^2 (T_{out} - T_{in})}. \tag{18}$$

$$= \tau_{eh} \tag{19}$$

where $m(\gamma) = \frac{4}{63}(-1+\gamma)^2(11+22\gamma-6\gamma^2+12\gamma^3)$ is a dimensionless constant resulting from the integration of $\mu(z)$ (for the cyclones studied here: $0.34 \le m(\gamma) \le 0.56$).

d. Comparing the scalings

The timescales for each mechanism depend on parameters that may change from wake to wake. One way to understand which restratification mechanism dominates is to divide the timescales of these mechanisms. Comparing restratification by EBF to surface fluxes

$$\frac{\tau_{ebf}}{\tau_{sf}} = \frac{2C_{sst}}{\rho C_p} \frac{L_f|f|}{u_*^2 cos\theta}. \tag{20}$$

If $\frac{\tau_{ebf}}{\tau_{sf}} > 1$, surface fluxes dominate the restratification, and one can see that this occurs in very wide wakes with slow along track winds (large L_f and small $u_*^2 cos\theta$). EBF dominate for $\frac{\tau_{ebf}}{\tau_{sf}} < 1$. Similarly comparing surface fluxes and eddy buoyancy fluxes,

$$\frac{\tau_{sf}}{\tau_{eddy}} = \frac{\rho C_p g\alpha C_e}{0.2C_{sst}} \frac{H'H_{eddy}(T_{out}-T_{in})}{L_f^2|f|}. \tag{21}$$

Comparing EBF and eddy buoyancy fluxes

$$\frac{\tau_{ebf}}{\tau_{eddy}} = \frac{g\alpha C_e}{0.1} \frac{H'H_{eddy}(T_{out}-T_{in})}{L_f u_*^2 cos\theta}. \tag{22}$$

4. Results

To compare the restratification timescales in real hurricane wakes, the parameters from each cyclone wake (Table 1) are used in the scalings. The illustrative model parameters from Section 2 are also given. The resulting timescales for restratification of the surface layer with $H' = H_{out}$ are shown in Table 2 and Figure 5. τ_{ebf} and τ_{sf} are roughly the same magnitude in all cases (30-100 and 30-110 days respectively). To make a more direct comparison τ_{sf} has been doubled because it is an e-folding time, and the other restratification times represent the full recovery. Although τ_{ebf} is comparable to τ_{sf} the uncertainty in τ_{ebf} is the same size as the forcing. This uncertainty is due primarily to variability in $u_*^2 cos\theta$. τ_{eddy} is the slowest restratification timescale when $H' = H_{out}$ (110-300 days). Although, the simulated wake was intended to be similar to Hurricane Frances, the front width (L_f) is significantly narrower in the simulation than in the region of the wake chosen to estimate the parameters. This increases the buoyancy gradient, and the effects of MLEs. For comparison, an observed restratification time is estimated from SST images (six-29 days). It should be noted, however, that this observed restratification time may represent the restratification time for a depth much shallower than H_{out} since satellite SST only captures the skin temperature of the ocean. An observed restratification time for Hurricane Igor was not estimated because the wake of Hurricane Igor was crossed by Hurricane Otto on Oct. 8, 2010. The methods

Table 2. Restratification timescales for the surface layer. $H' = H_{out}$. The true restratification timescale as estimated from the satellite SST is given for comparison. Note: two e-folding times have been given for τ_{sf} to be more comparable to the other timescales.

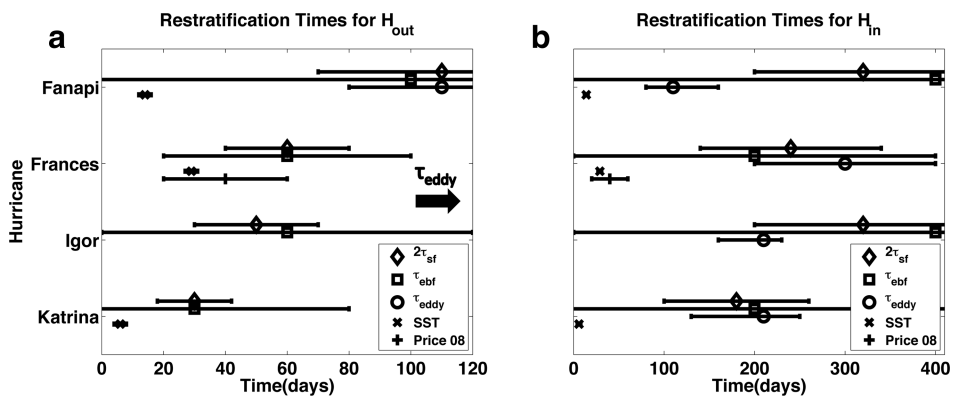| Cyclone	$\tau_{ebf}(days)$	$2\tau_{sf}(days)$	$\tau_{eddy}(days)$	$SST(days)$
Fanapi	100 ± 200	110 ± 20	110^{+50}_{-30}	14 ± 2
Frances	60 ± 40	60 ± 10	300 ± 100	29 ± 2
Igor	60 ± 60	50 ± 10	210^{+20}_{-50}	N/A
Katrina	30 ± 50	30 ± 6	210^{+40}_{-80}	6 ± 2
Model	48	60 ± 10	45	N/A

Figure 5. Restratification times for each cyclone. Error bars represent the 90% confidence interval. The Price et al. (2008) e-folding time has been doubled to compare more directly to the other times that represent full restratification.

for calculating this observed restratification time are discussed in Appendix A. Price et al. (2008) give a comparable restratification time of 40 ± 20 days for Hurricane Frances based solely on one-dimensional effects (Fig. 5).

The timescales for restratification of the surface layer with $H' = H_{in}$ are shown in Table 3 and Figure 5. τ_{ebf} and τ_{sf} both increase proportionately with depth (H') whereas τ_{eddy} is inversely proportional to depth. Thus, choosing a deeper restratification depth (H_{in}) lengthens τ_{ebf} and τ_{sf}, making all three timescales comparable. Although the scenario where the entire deeply mixed wake restratifies all at once seems unlikely given the model results (Section 2), when no sub-surface information is available, the $H' = H_{in}$ case is given as an upper bound on the depth that may be restratified. In addition, this case shows how sensitive the restratification times are to the wake parameters, and that even the wakes presented here exist in a parameter regime that is not too far from all restratification mechanisms being equal.

Table 3. Same as for Table 2 except $H' = H_{in}$.

Cyclone	$\tau_{ebf}(days)$	$2\tau_{sf}(days)$	$\tau_{eddy}(days)$	$SST(days)$
Fanapi	400 ± 600	320 ± 60	110^{+50}_{-30}	14 ± 2
Frances	200 ± 200	230 ± 50	300 ± 100	29 ± 2
Igor	400 ± 200	320 ± 60	210^{+20}_{-50}	N/A
Katrina	200 ± 300	180 ± 40	210^{+40}_{-80}	6 ± 2
Model	178	220 ± 40	46	N/A

Table 4. Restratification timescales for the subsurface bolus. $H' = H_{out}$. Note that the different columns have different units.

Cyclone	$\tau_{ev}(days)$	$\tau_{eh}(days)$	$\tau_{sb}(10^5 days)$	$\tau_{eh+ev}(days)$
Fanapi	500^{+200}_{-100}	$1,600^{+700}_{-400}$	$100,000 \pm 30,000$	400^{+200}_{-100}
Frances	$1,900 \pm 800$	$4,000 \pm 2,000$	8 ± 0.2	$1,300 \pm 500$
Igor	$1,500^{+200}_{-400}$	$2,700^{+300}_{-700}$	5 ± 0.2	$1,000^{+100}_{-200}$
Katrina	$1,400^{+200}_{-600}$	$3,000^{+500}_{-1,000}$	0.05 ± 0.03	$1,000^{+200}_{-400}$
Model	260	613	7	181

It is important to note that the timescales given here are long when compared to observed recovery timescales. This is in large part because each timescale is for one restratification mechanism alone. Also, recall that the timescales for surface fluxes in Figure 5 and Tables 2 and 3 are twice the e-folding time to better compare to the other timescales which are for a fully restored wake. To estimate a restratification timescale that combines the effects of multiple processes, one can sum the heat fluxes of the processes and compute an e-folding time. For example, considering the effects of the dominant processes in the $H' = H_{out}$ case (i.e. EBF and surface fluxes), one obtains,

$$\frac{\rho C_p}{C_{sst+ebf}} H' = \tau_{sf+ebf}, \tag{23}$$

where

$$C_{sst+ebf} = C_{sst} + \frac{u_*^2 cos\theta \rho C_p}{f L_f}. \tag{24}$$

In the case of Typhoon Fanapi, this gives an e-folding time of ~ 29 days, comparable to the observed e-folding time (23 days) given by Mrvaljevic et al. (2013).

The timescales for restratification in the sub-surface bolus are given in Table 4. As expected the eddy buoyancy fluxes (τ_{eh} and τ_{ev}) are much more effective than the shortwave penetrating solar radiation (τ_{sb}), with vertical eddy buoyancy fluxes faster than horizontal $\left(\tau_{eh} = \frac{1}{m(\gamma)} \tau_{ev}\right)$. However, the combined effect of vertical and horizontal eddy buoyancy

fluxes gives timescales for restratification that are multi-year for all cyclones (400–1,300 days). Thus, it is likely that much of the remaining sub-surface bolus is engulfed by the deepening of the wintertime mixed layer before the eddies have time to transport it away or the solar fluxes have time to heat it up.

The potential for climatic impacts is investigated by comparing H_{in} to the maximum (wintertime) climatological mixed layer depth (MLD_w, described in Appendix A) in each of the hurricane regions . In every case $H_{in} > MLD_w$, which, together with the long eddy timescales suggests that these cyclones injected some heat into the permanent thermocline, which may affect the ocean heat transport. However, MLD_w is a monthly climatology that gives the average mixed layer depth for each month, so this may not be representative of the maximum mixed layer depth. To verify whether the sub-surface bolus is completely eliminated by wintertime mixed layer deepening, one would need in-situ measurements of the wake region through the wintertime. Regardless of how much of the bolus is eliminated by the wintertime mixed layer deepening, the timescale to transport the heat any appreciable distance by subduction and meridional overturning is far slower than the timescale for restratification by the MLEs which continue to act toward eliminating the bolus until no stratification anomaly remains.

5. Summary and conclusions

The basic restratification mechanisms for a cold hurricane wake were reviewed and estimated. The different sizes and strengths of four specific cyclone wakes and one simulated wake were used to see the variability across different wake parameters.

The EBF and surface fluxes restratify at roughly the same rate, although while the EBF restratifies one side of the wake, it simultaneously destratifies the other. Thus, the Ekman flow advects the upper part of the cold wake away from the lower part that is too deep to be effected by EBF. While this mechanism looks ineffective from one in the reference frame moving at the Ekman flow velocity, capping the deep bolus of the wake prevents surface fluxes and EBF from restratifying the bolus. EBF also makes the wake restratification asymmetrical, which creates an interaction with MLEs. Therefore, although EBF does not heat the wake, this two-dimensional mechanism affects wake restratification in profound ways that can not be captured by one-dimensional physics alone. Furthermore, the real Ekman flow includes vertical shear which would result in greater buoyancy fluxes at the top of the mixed layer, thus restratifying it. One-dimensional surface fluxes will dominate only if the wake is wide and the restratifying layer is thin. If the wake is relatively narrow, and the restratifying layer is very deep, three-dimensional MLEs dominate. Dominance of the surface restratification by three-dimensional physics was not estimated for the parameters for any of the cyclones examined here. However, in a late season cyclone or one with a pathway other than those examined here, deeper mixed layers would have strengthened the effects of MLEs. Thus, two-dimensional and three-dimensional mechanisms may contribute at a level rivaling the one-dimensional mechanisms. The scalings presented here are useful in determining the relative contributions for a variety of wake parameters.

The subsurface bolus is acted upon by essentially only MLE buoyancy fluxes. For the parameters of the cyclones studied here, the timescales associated with the removal of the bolus are multi-year. Thus, it is expected that wintertime deepening of the mixed layer will engulf at least a portion of the bolus before this eddy-based recovery. If the bolus is not rapidly subducted into the deeper thermocline, MLEs will continue to erode that stratification anomaly over the following year, where it can be eliminated by wintertime deepening.

APPENDIX

A. Data collection methods

Using the NOAA Historical Hurricane Tracks (http://csc.noaa.gov/hurricanes), cyclones were located. Data were then obtained from NOAA OceanWatch Delayed, Science-Quality Satellite Data for the Sea Surface Temperature Multi-Satellite Blended Product (blending Moderate Resolution Imaging Spectroradiometer (MODIS) on Aqua, Advanced Very High Resolution Radiometer (AVHRR) on POES-17 and POES-18, Imager on GOES-10 and GOES-12, and the Advanced Microwave Scanning Radiometer (AMSR-E) on Aqua) (http://las.pfeg.noaa.gov/oceanWatch). This data product has global coverage at 0.1 degree resolution from July 4, 2002 to the present. When an easily visible wake was found in SST images, the satellite SST data from a few days before and several days after the wake were obtained. For each day, a mask was made to establish which locations were inside the wake and which constituted the left and right sides of the wake (e.g. Hurricane Igor, Fig. 6). Cross track lines of SST are averaged, and these cross track profiles are resampled using bootstrapping to give a 90% confidence interval. The maximum temperature is picked at the location on the left side of the wake where the mean temperature profile appears to have mostly leveled off. It should be noted that the cross track temperature profile never completely flattens because there is some temperature change in the cross track direction due to change in latitude. The minimum of the along-track line in the center of the wake is used to get the maximum possible temperature gradient, and the 90% confidence interval is computed (again with bootstrapping). The front width of the wake (L_f) is defined to be the distance between the point that is sampled to obtain T_{out}, and the point sampled to obtain T_{in}. Similarly, the error in L_f is taken to be the distance between the mean cross track temperature profile, and the temperature profile given by the 90% confidence interval (Fig. 7). The modeled wake parameters were sampled in the same fashion except that confidence
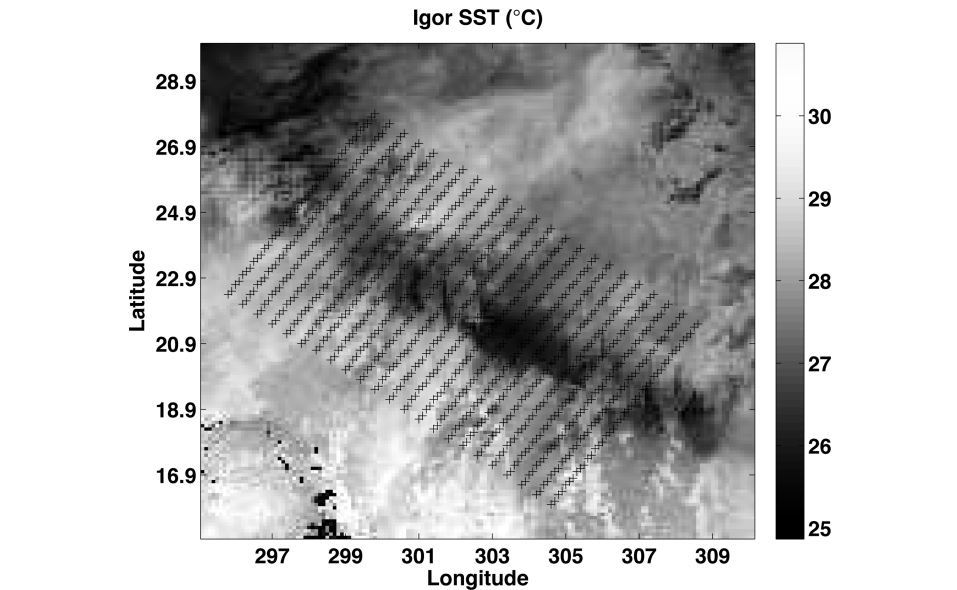
Igor SST (°C)

Figure 6. SST on Sept. 19, 2010, ≈ two days after Igor passed over the region. The cross-track lines where the temperature is sampled are shown.
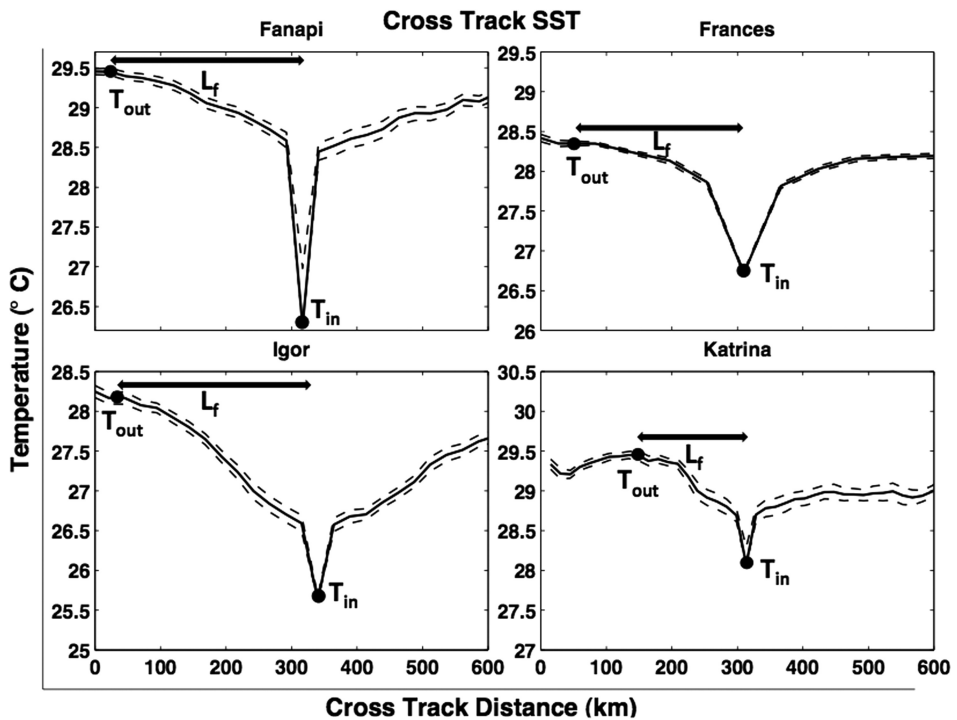
Cross Track SST

Figure 7. Cross-track SST profile from the average (solid lines) of the cross-track lines as in Figure 6. Distance shown is the distance from the left-most sampled spot. The dashed lines indicate the 90% confidence interval. Note the colder SSTs right of the wake.

intervals are not estimated since in the cases of the real wakes, the confidence intervals come from along track variability which is not present in the model. Treating the wake as a simple temperature drop ($T_{out} - T_{in}$) across L_f is treating the cross track temperature profile as linear when one can see from Figure 7 that it is clearly not linear. A hyperbolic tangent profile was also considered and resulted in O(1) changes to the scalings.

Wind stress data were taken from ERA Interim Re-Analysis (http://data-portal.ecmwf.int/data/d/interim_daily/). These data were interpolated to the SST grid, and averaged in space over the same mask as for the SST. They are then averaged in time over a month (10 days for Igor to avoid anomalous winds around the time of Hurricane Otto) of the recovery, and a standard deviation is obtained. Two standard deviations are used as the uncertainty, and the mean and uncertainty are divided by an assumed water density of 1,025 $kg\ m^{-3}$ to give u_*^2.

Approximate observed restratification times have been determined using the method described above. The method for judging whether the SST has recovered is to compare the cross track SST on each day to a five year climatology (for each of the two months in which the recovery occurs) of the SST which has been sampled and averaged in the same way as the cross track SST (Fig. 8). The SST is determined to have recovered when the cross track SST profile has approximately (determined by eye) the same slope as the climatology for either of the two months of the hurricane recovery period.

The mixed layer depths outside the cold wake (H_{out}) for cyclones Fanapi, Frances and Igor were found from the OCCA mean monthly temperature climatology, which is derived from drifter and satellite data from Dec. 2003 through Nov. 2006 (Forget, 2010). The World Ocean Atlas climatology (Levitus, 1982) was used for Hurricane Katrina since the OCCA climatology does not have values in the Gulf of Mexico. The mixed layer depths outside the wake (H_{out}) were determined by using the 0.2°C rule, which states that the mixed layer depth is the depth at which the ocean temperature is 0.2°C cooler than the surface temperature (de Boyer Montégut et al., 2004). The mixed layer depths inside the wake (H_{in}) were calculated by averaging the climatological profile down to some depth level (to represent mixing) until the average temperature is 0.1°C cooler than T_{in} (thus, assuming a linear decrease, the base of the mixed layer would be 0.2°C cooler than the surface).

$$\frac{1}{H_{in}} \int_{-H_{in}}^{0} T\,dz = T_{in} - 0.1 \tag{25}$$

Discretizing for observed data, and solving for H_{in} gives,

$$\frac{\sum_{n=0}^{N} T_n \Delta z_n}{(T_{in} - .1)} = H_{in}. \tag{26}$$

The wintertime mixed layer depth (MLD_w) is based on a global two degree resolution climatology of mixed layer depth (de Boyer Montégut et al., 2004). The same 0.2 degree
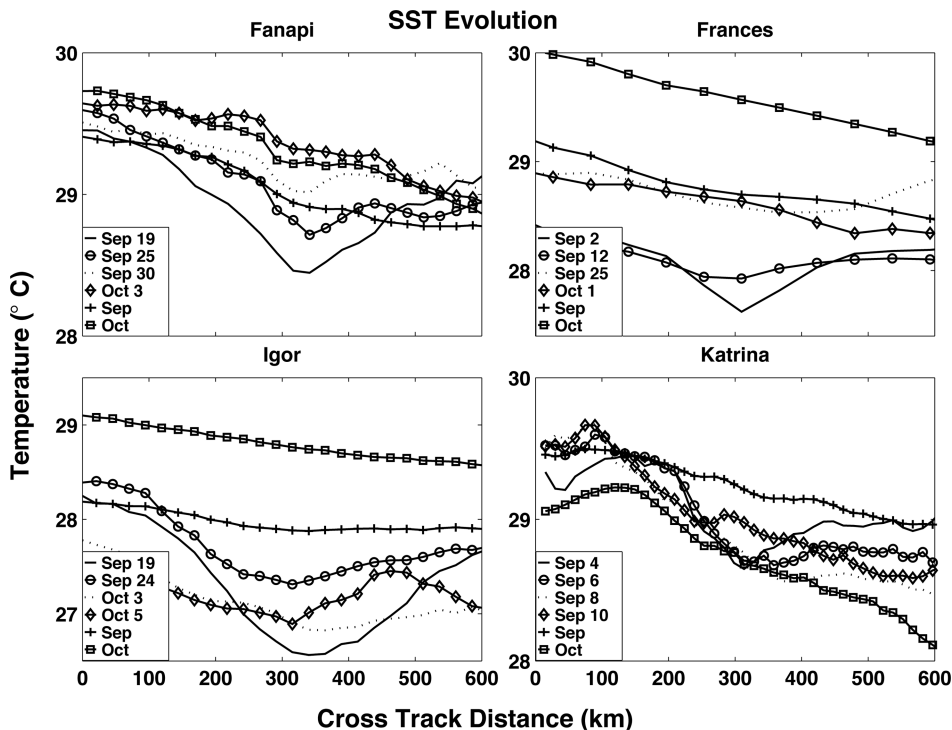
Figure 8. Time Evolution of the cross-track SST profile from which the approximate recovery time
is determined. "Sept." and "Oct." are five year climatologies. Note: the temperature scales differ,
but all temperature scales span $2°C$.

rule, as above, is used as a threshold temperature change from the surface to the mixed layer
depth. In some cases a density change threshold of 0.03 $kg\ m^{-3}$ is used instead. The grid
points nearest to the centers of the respective hurricane wakes are chosen for the MLD_w
estimate.

B. A Note on restratification depth

As stated in Section 3a, the approach is to obtain bounds on the restratification depth (H').
H_{out} is chosen as the lower (shallower) bound, and H_{in} is chosen as the upper (deeper)
bound, and methods for calculating these are discussed in Appendix A. It is clear from
the simulations presented in Section 2, that the quickly restratifying surface layer is no
deeper than H_{in}. However, one might expect the lower bound on restratification depth to
be shallower than the climatological depth used (H_{out}). Two potential choices for a lower
bound are the Monin-Obukhov Depth (H_{mo}), and a mixed layer depth (H_{kt}) defined by
Kraus and Turner (1967).

Monin and Obukhov (1954) defined a length scale for boundary layer turbulence as

$$H_{mo} \equiv \frac{\rho C_p T u_*^3}{kgq}, \tag{27}$$

where q is the heat flux and k is the Von Kármán constant ($k \approx 0.41$). Applying the hurricane wake parameters to (27) gives

$$H_{mo} = \frac{\rho C_p T_{in} u_*^3}{kg(-Q_{out} + C_{sst}(T_{out} - T_{in}) + S_0 I_2)}, \tag{28}$$

where $S_0 I_2$ is an approximation to the $S_{H'}^0$ term in the in-wake heat flux Equation 3. Although this approximation overestimates the effect of stratification thus decreasing H_{mo}, this is consistent with the goal of obtaining a lower bound for restratification depth. H_{mo} requires that the production of turbulent kinetic energy (TKE) by shear to be balanced by that of buoyancy. As with the heat flux balance, it is assumed that outside the wake the TKE production terms are in equilibrium, thus $H_{out} = H_{mo}$, but during the evolution of a cold wake, this balance may not exist. If this balance did exist in the cold wake, one would expect H_{mo} to be shallower in the wake than it is outside due to reduced latent and sensible heat loss (the $C_{sst}(T_{out} - T_{in})$ term). In (28) the only two terms that may change to achieve this balance are u_* and T_{in}, and it is unreasonable to assume that the wind field is determined exclusively by the local SST. This precludes the possibility that these two quantities evolve exactly so as to maintain this balance between shear and buoyancy TKE production. Additionally, since H_{mo} will vary with both u_* and T_{in}, using the mean of u_* over any period of time does not provide a good measure of the mean of H_{mo}. To determine a good mean of H_{mo}, one would also need to know the evolution of temperature. To know the evolution of temperature requires knowing H_{mo}, and although one could evolve both by coupling the time derivative of (28) with (3), recall that the solar penetration term in (3) involves an exponential of H_{mo}. This term requires that the proposed coupled system of equations be solved numerically. Numerical modeling is avoided here, as the goal of this work is to develop simplified scalings that describe separately the restratification mechanisms, and how they relate to the wake parameters. It should be noted here that the mixing schemes in numerical models (e.g. KPP, PWP) do maintain a similar balance of TKE production by shear and by buoyancy to establish a mixing depth when in this forcing regime.

H_{kt} is based on heat and energy budgets derived by Kraus and Turner (1967). Kraus and Turner (1967) begin with a heat budget identical to (3) except with the addition of an entrainment term. This along with an energy budget yields two possible depths

$$H_{kt} \equiv \frac{\frac{C_p}{g\alpha} u_*^3 - D + \frac{S_0 I_2}{k_2}}{Q_{out} + C_{sst}(T_{out} - T_{in}) + S_0 I_2}, \tag{29}$$

if one assumes the temperature is in steady state, or $2H_{kt}$ if one assumes that the mixed layer base is shoaling. Here, D is an energy dissipation term which is assumed to be negligible.

Assuming this thin restratifying layer is as in the model results (Fig. 3), then the mixed layer base would need to deepen, not shoal, to return to pre-hurricane conditions. The assumption of steady state temperature is not very reasonable either because the goal is to obtain a timescale over which the temperature warms to pre-hurricane conditions. These assumptions and others made by Kraus and Turner (1967) are more appropriate when considering the evolution of the mixed layer on seasonal timescales (which was precisely their goal). Furthermore, determining a single H_{kt} by a time mean has the same problems as in the H_{mo} case.

Finally, it is important to note that the particular choice of H' does not influence the dependence of the scalings on depth. That is to say the forms of (7) and (11) do not change with different choices of H', but of course the values of each will change. The choices of H' discussed above are simply guidelines for what might be good bounds on restratification depth.

C. Error propagation

Uncertainties in T_{in}, T_{out}, L_f, and $u_*^2 cos\theta$ (given in Table 1) are propagated through the expressions for each timescale to obtain estimates of the error in each timescale. In general, the error propagation is calculated as follows

$$\delta\tau^2 = \sum_{n=1}^{N} \left(\frac{\partial\tau}{\partial x_n} \delta x_n \right)^2, \tag{30}$$

where each timescale, τ, is a function of N variables, x_n, each with error δx_n. So for example,

$$\delta\tau_{eddy}^2 = \left(\frac{\partial\tau_{eddy}}{\partial L_f} \delta L_f \right)^2 + \left(\frac{\partial\tau_{eddy}}{\partial T_{out}} \delta T_{out} \right)^2 + \left(\frac{\partial\tau_{eddy}}{\partial T_{in}} \delta T_{in} \right)^2, \tag{31}$$

thus,

$$\delta\tau_{eddy}^2 = \tau_{eddy}^2 \left[\left(\frac{\delta L_f}{L_f} \right)^2 + \left(\frac{\delta T_{out}}{(T_{out} - T_{in})} \right)^2 + \left(\frac{\delta T_{in}}{(T_{out} - T_{in})} \right)^2 \right]. \tag{32}$$

Since the goal here is to give an upper and lower bound for restratification depth (H_{out} and H_{in}), uncertainty is not calculated for these assumed depths, as the range of possible depths itself provides the uncertainty in restratification timescales. If one were to calculated these timescales for a hurricane wake where subsurface information was available, and a single restratification depth could be estimated, then the uncertainty of that estimate would be taken into account.

D. Validation of the mixed layer eddy parameterization for the hurricane wake

Figure 9 shows that the eddy parameterization (Section 3c, Fox-Kemper et al., 2008) does a good job at estimating the initial rate of eddy restratification when compared to the
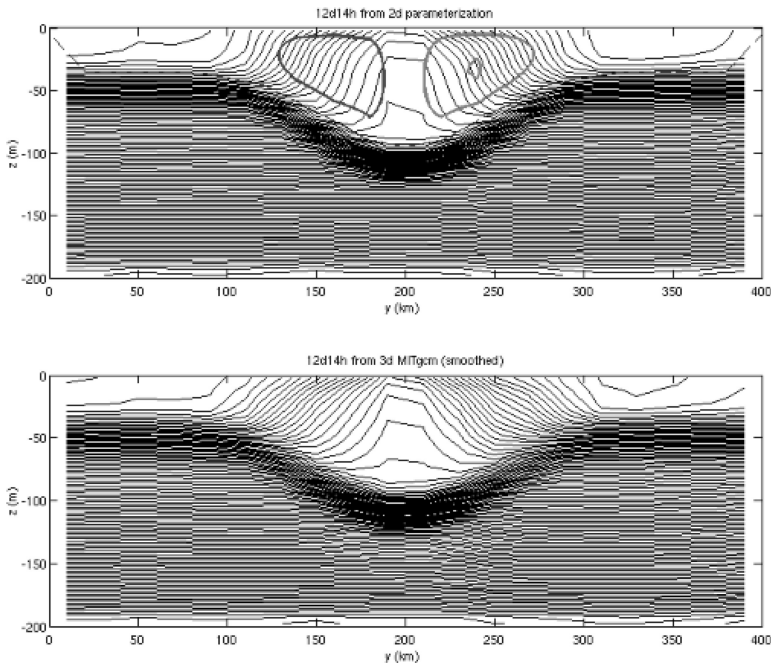
Figure 9. Restratification of an idealized hurricane wake in the absence of external restratification. The upper panel shows the resulting buoyancy structure (thin contours) after 12.5 days of restratification in a two-dimensional simulation using the MLE parameterization. The thicker contours show the instantaneous eddy-induced streamfunction from (8). The lower panel shows the along-wake mean buoyancy from the three-dimensional simulation with explicitly resolved MLEs of Figure 4.

model with no other restratification processes (upper panel of Fig. 4). The restratifying wake problem is somewhat different from the single mixed layer front problem over a flat mixed layer base studied by Fox-Kemper et al. (2008). However, the agreement in the location of isopycnals and slope of Figure 9 indicates that the same scaling (8) applies here as well. Apparently the two fronts on either side of the wake are quasi-independent, and the tilted mixed layer base is not sufficient to upset the parameterization. Boccaletti et al. (2007) show that a mixed layer base tilt of 5% minimally affects mixed layer instabilities; here the tilt grade is only 0.05%. Experimentation indicates that the mixed layer depth relevant for the MLE restratification rates is near $H_{eddy} \approx \frac{1}{2}(H_{in} + H_{out})$, and this choice greatly simplifies computing the restratification rate.

After this time period, when the remnant cold wake becomes an interior bolus of destratified fluid, the eddy restratification continues by skew fluxes of buoyancy that serve to spread the destratified fluid along isopycnals into the more stratified water to either side. Note that in terms of the skew fluxes, $(\overline{\mathbf{u}'b'} = \mathbf{\Psi} \times \nabla \bar{b})$, the contours of $\mathbf{\Psi}$ in Figure 9 serve as bullseyes circling the region where the skew fluxes are greatest.

REFERENCES

Adcroft, A.; J. M. Campin; S. Dutkiewicz; C. Evangelinos; D. Ferreira; G. Forget; B. Fox-Kemper; P. Heimbach; C. Hill; E. Hill, et al. 2008. The mitgcm user manual.

Bachman, S. and B. Fox-Kemper. April 2013. Eddy parameterization challenge suite. I: eady spindown. Ocean Modelling, *64*, 12–28.

Boccaletti, G.; R. Ferrari and B. Fox-Kemper. 2007. Mixed layer instabilities and restratification. Journal of Physical Oceanography, *37*(9), 2228–2250.

Cornillon, P.; L. Stramma and J. F. Price. March 1987. Satellite measurements of sea-surface cooling during Hurricane Gloria. Nature, *326*(6111), 373–375.

D'Asaro, E. A.; T. B. Sanford P. P. Niiler and E. J. Terrill. 2007. Cold wake of hurricane frances. Geophysical Research Letters, *34*(15).

de Boyer Montégut, C.; G. Madec; A. S. Fischer; A. Lazar and D. Iudicone. 2004. Mixed layer depth over the global ocean: An examination of profile data and a profile-based climatology. Journal of Geophysical Research: Oceans (1978–2012), *109*(C12).

Emanuel, K. July 2001. Contribution of tropical cyclones to meridional heat transport by the oceans. Journal of Geophysical Research-Atmospheres, *106*(D14), 14771–14781.

Forget, G. June 2010. Mapping ocean observations in a dynamical framework: A 2004-06 ocean atlas. Journal of Physical Oceanography, *40*, 1201–1221.

Fox-Kemper, B. and D. Menemenlis. 2008. Can large eddy simulation techniques improve mesoscale rich ocean models? Geophysical Monograph Series, *177*, 319–337.

Fox-Kemper, B.; G. Danabasoglu; R. Ferrari; S. M. Griffies; R. W. Hallberg; M. M. Holland; M. E. Maltrud; S. Peacock and B. L. Samuels. 2011. Parameterization of mixed layer eddies. iii: Implementation and impact in global ocean climate simulations. Ocean Modelling, *39*(1-2), 61–78.

Fox-Kemper, B. and R. Ferrari. 2008. Parameterization of mixed layer eddies. Part II: Prognosis and impact. Journal of Physical Oceanography, *38*(6), 1166–1179.

Fox-Kemper, B.; R. Ferrari and R. Hallberg. 2008. Parameterization of mixed layer eddies. Part I: Theory and diagnosis. Journal of Physical Oceanography, *38*(6), 1145–1165.

Gnanadesikan, A. and W. G. Anderson. February 2009. Ocean water clarity and the ocean general circulation in a coupled climate model. Journal of Physical Oceanography, *39*(2), 314–332.

Huang, P.; T. B. Sanford and J. Imberger. 2009. Heat and turbulent kinetic energy budgets for surface layer cooling induced by the passage of hurricane frances (2004). Journal of Geophysical Research: Oceans (1978–2012), *114*(C12).

Jansen, M.; R. Ferrari and T. Mooring. 2010. Seasonal versus permanent thermocline warming by tropical cyclones. Geophys. Res. Lett., *37*, L03602.

Jerlov, N. G. 1957. *Optical studies of ocean waters*, volume 3. Elanders boktr.

Korty, R. L.; K. A. Emanuel and J. R. Scott. 2008. Tropical cyclone-induced upper-ocean mixing and climate: Application to equable climates. Journal of Climate, *21*, 638–654.

Kraus, E. and J. Turner. Feb 1967. A one-dimensional model of the seasonal thermocline ii. the general theory and its consequences. Tellus, *19*, 98–106.

Large, W. G.; J. C. McWilliams and S. C. Doney. November 1994. Oceanic vertical mixing - a review and a model with a nonlocal boundary-layer parameterization. Reviews of Geophysics, *32*(4), 363–403.

Large, W. and S. Yeager. 2012. On the observed trends and changes in global sea surface temperature and air-sea heat fluxes (1984–2006). Journal of Climate, *25*(18), 6123–6135.

Levitus, S. E. 1982. *Climatological atlas of the world ocean*. NOAA Professional Paper 13, US Government Printing Office, Washington DC, 173.

Mahadevan, A.; A. Tandon and R. Ferrari. 2010. Rapid changes in mixed layer stratification driven by submesoscale instabilities and winds. J. Geophys. Res., *115*, C03017.

McClean, J. L.; D. C. Bader; F. O. Bryan; M. E. Maltrud; J. M. Dennis; A. A. Mirin; P. W. Jones; Y. Y. Kim; D. P. Ivanova; M. Vertenstein, et al. 2011. A prototype two-decade fully-coupled fine-resolution ccsm simulation. Ocean Modelling, *39*(1), 10–30.

Monin, A. and A. Obukhov. Oct 1954. Basic laws of turbulent mixing in the surface layer of the atmosphere. Tr. Akad. Nauk SSSR Geophiz. Inst., *24*(151), 163–187.

Mrvaljevic, R.; P. Black; L. Centurioni; Y.-T. Chang; E. D'Asaro; S. Jayne; C. Lee; R.-C. Lien; I.-I. Lin; J. Morzel; P. N. (deceased); L. Rainville and T. B. Sanford. 2013. Evolution of the cold wake of typhoon fanapi. Geophys. Res. Lett., *40*.

Pasquero, C. and K. Emanuel. January 2008. Tropical cyclones and transient upper-ocean warming. Journal of Climate, *21*(1), 149–162.

Price, J. F. 1981. Upper ocean response to a hurricane. Journal of Physical Oceanography, *11*, 153–175.

Price, J. F.; R. A. Weller and R. Pinkel. July 1986. Diurnal cycling: Observations and models of the upper ocean response to diurnal heating, cooling, and wind mixing. Journal of Geophysical Research-Oceans, *91*(C7), 8411–8427.

Price, J. F.; J. Morzel and P. P. Niiler. July 2008. Warming of SST in the cool wake of a moving hurricane. Journal of Geophysical Research-Oceans, *113*(C7).

Sullivan, P. P.; L. Romero; J. C. McWilliams and W. Kendall Melville. 2012. Transient evolution of langmuir turbulence in ocean boundary layers driven by hurricane winds and waves. Journal of physical oceanography, *42*(11), 1959–1980.

Tandon, A. and C. Garrett. 1994. Mixed layer restratification due to a horizontal density gradient. Journal of Physical Oceanography, *24*, 1419–1424.

Tandon, A. and C. Garrett. 1995. Geostrophic adjustment and restratification of a mixed layer with horizontal gradients above a stratified layer. Journal of Physical Oceanography, *25*, 2229–2241.

Thomas, L. N. 2005. Destruction of potential vorticity by winds. Journal of Physical Oceanography, *35*, 2457–2466.

Thomas, L. N. and C. M. Lee. 2005. Intensification of ocean fronts by down-front winds. Journal of Physical Oceanography, *35*, 1086–1102.

Thomas, L. N. and R. Ferrari. NOV 2008. Friction, frontogenesis, and the stratification of the surface mixed layer. Journal of Physical Oceanography, *38*(11), 2501–2518.

Vincent, E. M.; G. Madec; M. Lengaigne; J. Vialard and A. Koch-Larrouy. 2012. Influence of tropical cyclones on sea surface temperature seasonal cycle and ocean heat transport. Climate Dynamics, pages 1–20.

Zedler, S. E.; P. P. Niiler; D. Stammer; E. Terrill and J. Morzel. April 2009. Ocean's response to hurricane frances and its implications for drag coefficient parameterization at high wind speeds. Journal of Geophysical Research-Oceans, *114*.